Vector soliton associated with polarization modulational instability in the normal-dispersion regime

M. Haelterman and A. P. Sheppard
Optical Sciences Centre, Australian National University, Canberra, Australia
(Received 21 September 1993)

We investigate the dynamics of the coupled nonlinear Schrödinger equations which describe light propagation in isotropic Kerr media including polarization effects. It is shown that the phenomenon of polarization modulational instability in the normal-dispersion regime is associated with the existence of a novel type of dark vector soliton. This soliton constitutes a localized structure separating adjacent domains of orthogonal polarization eigenstates of the Kerr medium and can be viewed as a polarization domain wall.

PACS number(s): 42.81.Dp, 42.81.Gs, 03.40.Kf

I. INTRODUCTION

Modulation instability (MI) is a general characteristic of wave propagation in nonlinear dispersive media and is of common occurrence in such diverse fields as plasma physics [1], fluid dynamics [2], and nonlinear optics [3]. It refers to the physical process in which a weak periodic perturbation of a uniform intense carrier wave grows exponentially as a result of the interplay between dispersion and nonlinearity. In the context of optics special attention has been paid to MI in Kerr media (e.g., optical fibers) in which light-wave propagation is described, in the scalar approximation of the electromagnetic field, by the nonlinear Schrödinger (NLS) equation [4,5]. In this approximation MI, which results from the interplay between self-phase-modulation and dispersion, requires anomalous group-velocity dispersion [6]. This condition is also necessary for the existence of bright solitons which result from an exact balance between nonlinearity and dispersion [4]. Using direct substitution methods, Akhmediev and co-workers developed an analytical approach to MI of the NLS equation [7,8]. A general three-parameter family of first-order solutions to the NLS equation was given that includes space- and time-periodic, stationary periodic, and solitary-wave solutions [8]. In this way, a direct and explicit link between MI and the fundamental bright NLS soliton was established for the first time.

When accounting for the polarization of the electromagnetic field, light propagation in isotropic Kerr material is described by two incoherently coupled NLS equations [3]. It is known since the early study of Berkhoer and Zakharov in the context of plasma physics [9] that incoherent coupling between two NLS equations leads to an extension of the frequency domain of MI to the normal dispersion regime. The physical mechanism behind incoherent coupling is cross-phase-modulation (XPM), which refers, in this case, to each polarization component modulating the phase of the other. XPM is a general phenomenon characteristic of the simultaneous nonlinear propagation of several waves belonging to different optical modes [3]. It was shown, in the context of fiber optics, that MI with normal dispersion can also occur through XPM between waves of different frequencies [10]. The author of this latter work foresaw the fundamental importance of this phenomenon when he conjectured that a soliton must exist that is associated with MI in the normal-dispersion regime in the same way as the bright NLS soliton is associated with MI for anomalous dispersion. The aim of this paper is to confirm the existence of this soliton. Note that throughout the paper we use the common colloquial term "soliton" for what should be more rigorously called a stationary solitary wave. Analogously to what is done in Ref. [8] for the single NLS equation, we establish a direct link between XPM-induced MI in the normal-dispersion regime and the associated soliton. The incoherently coupled NLS equation being nonintegrable, most of our developments are based on numerics, although an approximate analytical approach to the problem is used as a guide in the search for new solutions. For the sake of simplicity we only consider the case of orthogonally polarized waves propagating in isotropic Kerr media. Our results, however, are relevant to other physical situations involving XPM between two optical modes.

The soliton associated with polarization modulational instability (PMI) in the normal-dispersion regime consists of a bound pair of solitary waves of orthogonal polarization and is, in this case, analogous to the so-called vector solitons or solitary waves recently reported in the literature. The idea that nonlinear coupling between optical modes could lead to the formation of a bound pair of solitary waves belonging to two different modes was first considered by Christodoulides and Joseph [11] and independently by Tratnik and Sipe [12]. These authors showed that stationary bound states of two orthogonally polarized bright solitons can propagate in birefringent Kerr materials in the anomalous dispersion regime. This type of solution to the coupled NLS equations was later analyzed in terms of bifurcations of polarized bright solitons [13,14] and their stability was investigated [15]. We have shown in a recent work that in fact linear birefringence is not necessary for such bound soliton states to exist [16,17]. Considering normal dispersion,

Christodoulides verified that the coupling of bright and dark NLS solutions may also result from the interplay between linear birefringence and XPM [18]. Coupled bright and dark NLS solitons were also predicted in the anomalous dispersion regime [18] but are inherently unstable [19]. Trillo *et al.*, showed that, using two waves of different wavelength situated below and above the zero-dispersion value, XPM can sustain propagation of a bright NLS soliton in the normal dispersion coupled to a dark NLS soliton in the anomalous dispersion [20]. This type of pairing of bright and dark solitons was later analyzed in more detail [21]. More recently, considering highly birefringent fibers in the anomalous dispersion, Tratnik found a new type of solitary waves that mix two polarization states but whose global behavior is governed by the scalar NLS equation [22]. Finally, Kivshar and Turitsyn showed the possibility of propagating bound states of gray solitons in the normal-dispersion regime [23]. To our knowledge this latter work and that of Ref. [18] constitute the only studies of vector bound solitary waves in the normal-dispersion regime. The existence of these vector solitary waves cannot be directly related to polarization modulational instability in the normal dispersion (contrary to what is suggested in Ref. [18]) and are therefore, in essence, fundamentally different from the vector soliton studied here.

The paper is organized as follows. In Sec. II we briefly recall the theory of polarized modulational instability in order to clearly establish the frame of our analysis. In Sec. III we develop an approximate model for the description of PMI and the periodic solutions of the coupled NLS equation. This model is based on the Fourier-mode truncation method used by Infeld for the study of Fermi-Pasta-Ulam recurrence in the NLS equation [24]. It provides a good and simple qualitative picture of the dynamics of the coupled NLS equations which allows us to establish a link between PMI and the existence of stationary periodic solutions to these equations. These solutions are equivalent to the so-called cnoidal waves [8] of the scalar NLS equation. Section IV is devoted to the numerical study of these stationary periodic solutions. We show that, like the scalar NLS cnoidal waves, these functions tend to a solitary-wave solution as their period tends to infinity. This solitary wave constitutes the soliton associated with PMI in the normal-dispersion regime. A detailed analysis of the soliton is given in Sec. V. Section VI is devoted to our conclusions.

II. POLARIZATION MODULATIONAL INSTABILITY

We consider one-dimensional propagation of polarized light in an isotropic dispersive Kerr material (e.g., a circular single-mode fiber). In dimensionless units the evolution of the circular polarization components is ruled by the incoherently coupled NLS equations [3]

$$i\frac{\partial E_+}{\partial z}-\frac{\sigma}{2}\frac{\partial^2 E_+}{\partial t^2}+\tfrac{1}{2}[(1-B)|E_+|^2+(1+B)|E_-|^2]E_+=0\ , \quad (1a)$$

$$i\frac{\partial E_-}{\partial z}-\frac{\sigma}{2}\frac{\partial^2 E_-}{\partial t^2}+\tfrac{1}{2}[(1-B)|E_-|^2+(1+B)|E_+|^2]E_-=0\ , \quad (1b)$$

where E_+ and E_- are the amplitudes of the counterrotating polarization components, z is the coordinate along the propagation axis, t is the time in the Gallilean reference frame traveling at the group velocity of the waves, σ is the sign of dispersion, $\sigma=+1$ ($\sigma=-1$) represents normal (anomalous) dispersion, and the coefficient $B=\chi^{(3)}_{1221}/\chi^{(3)}_{1111}$, where $\chi^{(3)}_{ijkl}$ is the nonlinear susceptibility tensor of the material [25]. Note finally that Eqs. (1) can be applied to the spatial domain by simply replacing the time t by the transverse coordinate of a two-dimensional diffractive Kerr cell. In that case Eqs. (1) describe the propagation of a laser beam in a self-focusing, $\sigma=-1$, or self-defocusing, $\sigma=+1$, Kerr medium.

Since the pioneering work of Berkhoer and Zakharov [9], MI of Eqs. (1) and generalized forms has been extensively studied in the literature (see, e.g., Refs. [3,10,26]). For the sake of clarity, we only give here the main steps of the developments of the linear stability analysis for the problem of interest to us, namely, the stability of a linearly polarized continuous wave (cw). The linearly polarized cw solution to Eqs. (1) reads $E_+=E_-=E_0\exp(i|E_0|^2z)$. The stability of this solution against the growth of periodic perturbation is examined by introducing in Eqs. (1) the ansatz $E_\pm=(E_0+e_\pm)\exp(i|E_0|^2z)$, where $e_\pm$ is a first-order perturbation of the form $e_\pm=\varepsilon_\pm\exp(\lambda z)\cos(\Omega t)$. Linearizing with respect to $\varepsilon_\pm$ leads to a characteristic polynomial of the fourth degree in λ. Among the corresponding four eigenvalues λ_i only two are potentially unstable. They are

$$\lambda_1=\Omega\sqrt{-\sigma P_0-\Omega^2/4}\ , \quad (2a)$$

$$\lambda_2=\Omega\sqrt{\sigma BP_0-\Omega^2/4}\ , \quad (2b)$$

where P_0 is the normalized power of the initial cw polarization components $P_0=|E_0|^2$. The first eigenvalue λ_1 corresponds to MI in the anomalous dispersion regime, $\sigma=-1$. The gain maximum $\lambda_{1\max}=P_0$ is obtained at the frequency $\Omega_{1m}=(-2\sigma P_0)^{1/2}$. Note that this instability is independent of the coefficient B, i.e., it does not involve the tensor character of the Kerr nonlinearity. Moreover, the eigenvector associated with λ_1 at the optimal frequency Ω_{1m} has the form

$$v_1=(\mathrm{Re}(\varepsilon_+),\mathrm{Im}(\varepsilon_+),\mathrm{Re}(\varepsilon_-),\mathrm{Im}(\varepsilon_-))_{\lambda=\lambda_1}=(1,1,1,1)\ ,$$

which shows that, under the effect of the instability, both polarization components exhibit the same evolution. In other words, as is well known, MI of the coupled NLS equations in the anomalous dispersion regime does not involve any changes in the linear polarization state of the field and does not differ from MI in the scalar NLS equation. The theory of Ref. [8] can then be applied and, naturally, the soliton associated with this instability is the usual bright NLS soliton which represents here a pulse of constant and uniform linear polarization.

The situation is fundamentally different for the insta-

bility governed by the second eigenvalue λ_2. We see from Eq. (2b) that, contrary to MI of the scalar NLS equation, this instability only occurs in the normal dispersion, $\sigma=+1$. Its maximum gain is $\lambda_{2\max}=BP_0$, which corresponds to the optimal frequency $\Omega_{2m}=(2\sigma BP_0)^{1/2}$. The role of the coefficient B shows that MI, in this case, depends intrinsically on the tensor character of the Kerr nonlinearity. The smaller B, the smaller the MI gain and its optimal frequency. The instability disappears in the absence of nonlinear birefringence, i.e., when $B=0$ (e.g., for an electrostriction-induced Kerr nonlinearity). Another important difference with respect to the scalar MI is revealed by the analysis of the eigenvector associated with λ_2. At the optimal frequency Ω_{2m} this eigenvector has the form

$$v_2=(\mathrm{Re}(\varepsilon_+),\mathrm{Im}(\varepsilon_+),\mathrm{Re}(\varepsilon_-),\mathrm{Im}(\varepsilon_-))_{\lambda=\lambda_2}$$
$$=(1,1,-1,-1,)\ .$$

This indicates that MI induces the exponential growth of periodic perturbations of opposite sign in the two circular polarization components of the initial linearly polarized cw signal. As a consequence, one may expect that, up to the nonlinear stage of the evolution of MI, the envelopes of the two circularly polarized fields exhibit two identical but π out-of-phase periodic structures. Since this instability involves a change of the state of polarization of the field, it is called polarization modulation instability. An illustration of PMI is given in Fig. 1, which shows the evolution of the intensity profiles of the two components E_+ and E_- obtained by numerical simulation of Eqs. (1) for $B=\frac{1}{3}$. The initial conditions correspond to a linearly polarized cw field slightly perturbed by a periodic signal at the optimal frequency, $E_\pm(z=0,t)=1\pm\varepsilon\cos(\Omega_{2m}t)$, where $\varepsilon=10^{-3}$. Periodic boundary conditions are considered. As predicted from the linear stability analysis, we verify in Fig. 1 the formation of two π out-of-phase identical periodic structures in both polarization components. Note that this result is general and does not depend on the type of initial perturbations. For instance, when seeding PMI with a white noise, the spectral components of the noise at the optimal frequency are selected in both polarizations and, in agreement with the form of the eigenvector v_2, they grow with a phase of $\pi/4$ and $5\pi/4$ with respect to the initial cw signal, giving rise to π phase-shifted temporal structures.

Let us note finally that the linear stability analysis applied to continuous waves of pure circular polarization shows that such waves obey the dynamics of the scalar NLS equation and, in particular, are modulationally stable in the normal-dispersion regime.

III. TRUNCATED THREE-WAVE MODEL

For the scalar NLS equation a link between the bright soliton and MI was established thanks to the discovery of an analytical three-parameter family of first-order solutions that includes space- and time-periodic, stationary periodic, and solitary-wave solutions [8]. The link between MI and the bright NLS soliton can be viewed as follows. The dynamics of MI is described by the space- and time-periodic solutions of the family in a given range of the parameters. Varying the family parameters shows that stationary periodic solutions constitute limiting states of these complex solutions. Since the stationary periodic solutions have the form of the elliptic cosine function cn, they have been called cnoidal waves. As is well known, when increasing the period, say, T, of the elliptic cosine, this function tends to a periodic train of pulses whose envelope tends to the hyperbolic secant function. In such a way that, in the limit $T=\infty$, the elliptic cosine becomes the hyperbolic secant function [27] corresponding to the bright NLS soliton.

Ideally, in order to find the soliton associated with PMI we should look for a similar general family of solutions of the coupled NLS equation (1). Seeing the complexity of these equations as compared to the single NLS equation, this task appears rather difficult [e.g., contrary to the scalar NLS equation, Eqs. (1) are not integrable for $B\neq 0$ [14,28]]. Even a numerical approach to the problem, similar to the one originally applied to the NLS equation [7,29], would be difficult to develop without further information on the dynamical features of Eqs. (1). This is the reason why we propose here an approximate model for the dynamics of PMI in Eqs. (1). This model provides a simple qualitative picture of the dynamics of periodic solutions of the coupled NLS equations. In particular it reveals the existence of space- and time-periodic solutions as well as stationary periodic solutions. The predictions of this model are used in Sec. IV as a guide in the search for the exact stationary periodic solutions to Eqs. (1) by means of numerics.

Since the early work of Infeld on the theory of the Fermi-Pasta-Ulam recurrence in the NLS equation [24], it is known that much physical insight into the complex dynamics of MI can be obtained by means of the Galerkin approximation. For the NLS equation this approximation leads to a three-wave truncated model which

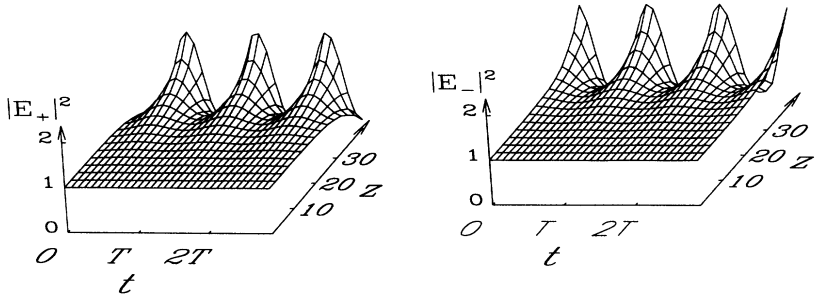

FIG. 1. Evolution of the intensity profiles of the two polarization components $E_\pm(z,t)$ of a initially linearly polarized cw field slightly perturbed by a periodic perturbation at the optimal frequency: $E_\pm(z=0,t)=1\pm10^{-3}\cos(\Omega_{2m}t)$ where for $B=\frac{1}{3}$, $\Omega_{2m}=0.816$, i.e., $T=7.7$. We clearly verify the formation of two identical but out-of-phase periodic structures in both circular polarization.

reduces the complexity of the dynamics to that of the conservation motion of a particle in a one-dimensional potential [30–32]. Three-wave truncated models were also proven to be efficient in the study of MI in nonlinear optical cavities described by driven and damped NLS equations [33–35]. The three-wave truncation approach to the problem of modulational instability in coupled NLS equations was first proposed in Ref. [36] for the study of nonlinear modulation of coupled waves in birefringent optical fibers. We show in the following that this approach is suitable to the study of the periodic solutions of Eqs. (1).

The stability analysis of Sec. II and more particularly the form of the eigenvector v_2, as well as the results of the numerical simulations illustrated in Fig. 1, suggest that it should be possible to describe PMI of Eqs. (1) by means of a three-mode Fourier truncation of the form

$$E_{\pm}(z,t)=E_0(z)\pm\sqrt{2}E_1(z)\cos(\Omega t)\ , \tag{3}$$

where Ω is the frequency of the temporal patterns. Naturally this truncation is only valid as long as higher harmonics do not significantly influence the system dynamics [24,30]. In order to ensure that higher harmonics are not linearly unstable we impose the condition $\Omega>\Omega_c/2$, where, according to Eq. (2b), $\Omega_c=2(BP_0)^{1/2}$ is the total PMI gain bandwidth or the PMI cutoff frequency (we set $\sigma=+1$ in the remaining of the paper). Note that in Eq. (3) we assume equal amplitudes for the two sideband waves [or Fourier components $\exp(i\Omega t)$ and $\exp(-i\Omega t)$]. In the following, we call E_0 and E_1 the amplitudes of the pump and the sideband waves, respectively. With the notation of Eq. (3) the power carried by each polarization component is given by $P=|E_0|^2+|E_1|^2$. It is important to note that the ansatz (3) is consistent with Eqs. (1) in the sense that the substitution of E_+ and E_- as given by Eq. (3) into Eq. (1a) (when neglecting all higher harmonics) leads to the same set of ordinary differential equations as the substitution of E_+ and E_- into Eq. (1b). This set is written as

$$i\frac{dE_0}{dz}+|E_0|^2E_0+(1-B)|E_1|^2E_0-BE_1^2E_0^*=0\ , \tag{4a}$$

$$i\frac{dE_1}{dz}+\tfrac{1}{2}\Omega^2E_1+(1-B)|E_0|^2E_1+\tfrac{3}{2}|E_1|^2E_1-BE_0^2E_1^*=0\ . \tag{4b}$$

Consequently, although the original model consists of two coupled NLS equations, the truncated model has a form analogous to that derived for the single NLS equation [24,30–32]. This result is important because it means that PMI can be described in terms of the dynamics of only two coupled Fourier modes. Moreover, it is easy to see from Eqs. (4) that the total power $P=|E_0|^2+|E_1|^2$ is a conserved quantity and that the power flow between the pump and sidebands only depends on their relative phase. Introducing the powers P_0 and P_1 and the phases ϕ_0 and ϕ_1 of the pump and sideband waves through the relations $E_0=(P_0)^{1/2}\exp(i\phi_0)$ and $E_1=(P_1)^{1/2}\exp(i\phi_1)$, we can then reduce the model to a set of two differential equations of the real variables P_1 and $\phi=\phi_0-\phi_1$.

$$\frac{dP_1}{dz}=2B(P-P_1)P_1\sin(2\phi)\ , \tag{5a}$$

$$\frac{d\phi}{dz}=-\tfrac{1}{2}\Omega^2+BP-2(B+\tfrac{1}{4})P_1+B(P-2P_1)\cos(2\phi)\ . \tag{5b}$$

These two self-consistent coupled real equations describe the physical content of the approximate model Eqs. (4) [i.e., the only information lost when deriving Eqs. (5) is the absolute phase of the field]. In order to investigate the existence of eigensolutions (or fixed points) and the dynamics of Eqs. (5), it is convenient to formulate the problem as a Hamiltonian system [36]. Introducing the normalized sideband power $\eta=P_1/P$, it is easy to see from Eqs. (5) that the variables η and ϕ are conjugate through the Hamiltonian

$$H=(\kappa-B)\eta+B(\eta-1)\eta\cos(2\phi)+(B+\tfrac{1}{4})\eta^2\ , \tag{6}$$

where $\kappa=\Omega^2/(2P)$, and thus obey the equations

$$\frac{d\eta}{d\xi}=\frac{\partial H}{\partial\phi},\quad \frac{d\phi}{d\xi}=-\frac{\partial H}{\partial\eta}\ , \tag{7}$$

where we introduced the scaled longitudinal coordinate $\xi=zP$. The dynamical features of PMI and, more generally, of the periodic solutions of the coupled NLS equations are qualitatively described by this simple one-dimensional Hamiltonian model. This model is remarkably similar to that derived in Refs. [30,31] for the study of MI and three-wave mixing in Kerr media in the scalar approximation. For a given Kerr material, i.e., for a given value of B, the Hamiltonian (6) has one degree of freedom determined by the parameter κ. In the following we consider the value $B=\frac{1}{3}$, which corresponds to the nonlinearity of optical silica fibers.

Following the ideology of Refs. [30–32,36], it proves convenient to characterize the dynamics by means of a phase-space representation. We consider the phase space of polar coordinates (η,ϕ) in such a way that the sideband power η and the relative phase ϕ are simply represented by the modulus and angle of the phase point, respectively. The origin of this plane represents therefore a linearly polarized continuous wave [i.e., $E_1=0$ in Eq. (3)]. The trajectories of Eqs. (6) and (7) are the contour lines of H in the phase space. They are plotted in Fig. 2 for the particular case of the optimal PMI frequency, i.e., $\kappa=\Omega_{2m}^2/(2P)=B$ [note that in Eqs. (2) the continuous-wave power P_0 is equal to the total power P since the sideband amplitude is assumed to be arbitrarily small in the stability analysis]. A simple glance at Fig. 2 allows us to see that the dynamical behavior of PMI is similar to that of MI in the scalar NLS equation, in particular, the instability of the cw signal (represented by the origin in the plane) corresponds to the presence of a hyperbolic unstable fixed point of the Hamiltonian system [36]. In other words, the system exhibits a homoclinic orbit characteristic of the Fermi-Pasta-Ulam recurrence in the NLS equation [24,30–32]. This orbit is a separatrix that divides the phase plane into two domains. The orbits of

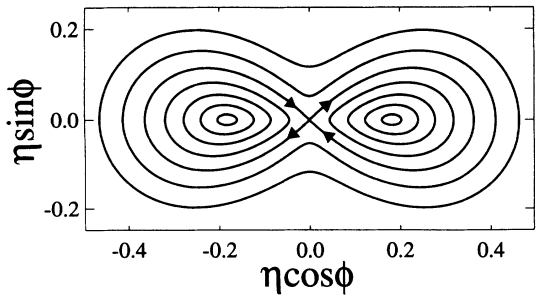

FIG. 2. Phase-space portrait of the dynamics of the space- and time-periodic solutions given by the approximate truncated Hamiltonian model for the optimal PMI frequency (i.e., $\kappa=B$). The orbits are the contour lines of the Hamiltonian H in polar coordinates (η,ϕ). We verify the existence of the homoclinic orbit corresponding to PMI of the linearly polarized cw signal. The arrows indicate the stable and unstable directions of the origin as obtained from the linear stability analysis of Sec. II.

these domains represent the two types of space- and time-periodic solutions of the coupled NLS equations (1) around the optimal frequency of PMI. Note that, in accordance with the ansatz (3), if a point (η,ϕ) running on an orbit represents the periodic evolution of one circular polarization component, say, E_+, then the point $(\eta,\phi+\pi)$ running on the corresponding symmetric orbit represents the evolution of the component E_-. The arrows on the separatrix orbit indicate the unstable directions of the origin (cw solution). The angles $\phi=\pi/4$ and $5\pi/4$ correspond naturally to the expression of the eigenvector v_2 obtained from the linear stability analysis.

We checked the validity of the truncated Hamiltonian model (6) and (7) by comparing its predictions with the results of direct numerical integration of the coupled NLS equations (1). For the sake of simplicity we set the total power P to unity in such a way that $\zeta=z$ and the comparison between both models is straightforward. Figure 3 shows the evolution in z of the intensity in $t=0$ of

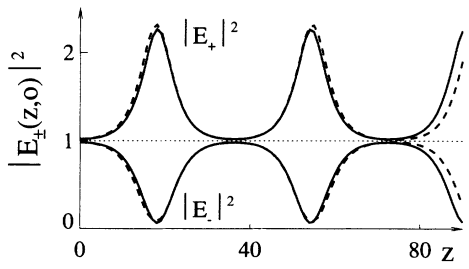

FIG. 3. Illustration of the Fermi-Pasta-Ulam recurrence associated with PMI. The solid lines show the evolution of the maximum and minimum, $|E_\pm(z,t=0)|^2$, of the intensity profiles of the polarization components given in Eq. (8). The initial conditions are $E_\pm(z=0,t)=1\pm\varepsilon\cos(\Omega t)$, where $\varepsilon=10^{-2}$ and $\Omega=1$. This evolution corresponds then to the inner orbits of the phase-space portrait which cross the axis $\eta\sin\phi=0$ at $\eta=\pm\varepsilon^2/2=\pm0.5\times10^{-4}$. The dotted curves show the result of direct numerical integration of Eqs. (1) (with $B=\frac{1}{3}$) with identical initial conditions. We verify a good qualitative agreement between both models.

both polarization components in the case of a continuous wave slightly perturbed by an amplitude modulation, i.e., with the initial conditions $E_\pm(z=0,t)=1\pm\varepsilon\cos(\Omega t)$, where $\varepsilon=10^{-2}$, and $\Omega=1$ ($\kappa=0.5$). The initial phase ϕ is then zero, which means that the evolution is described by an orbit inside the homoclinic separatrix. The solid curves in Fig. 3 give the intensities $|E_\pm(x,t=0)|^2$ obtained from the Hamiltonian model. Using the ansatz (3) and expressing it in terms of η and ϕ [whose evolution is given by Eqs. (7)], we find

$$|E_\pm(z,t=0)|^2=1+\eta(z)\pm2\sqrt{2[1-\eta(z)]\eta(z)}\cos[\phi(z)]\ . \quad (8)$$

The dotted curves are the result of numerical integration of Eqs. (1). We verify the validity of the predictions of the truncated model. In particular we observe that Eqs. (1) exhibit a recurrent behavior analogous to that of the scalar NLS equation. Figure 4 illustrates the recurrence for the two types of orbits shown in Fig. 2. It shows the evolution of the intensity profiles of both polarization components obtained by numerical integration of Eqs. (1). Figure 4(a) corresponds to the parameters of Fig. 3, whereas Fig. 4(b) corresponds to an outer orbit obtained with an initial phase $\phi(z=0)=\pi/2$, i.e., the initial conditions are $E_\pm(z=0,t)=1\pm i\varepsilon\cos(\Omega t)$ (with the same values of ε and Ω as above). A good qualitative agreement between Eqs. (1) and the truncated model has been observed as long as the frequency Ω is higher than half the PMI cutoff frequency, $\Omega>\Omega_c/2$. Let us note that the similarity with the scalar NLS dynamics is only qualitative. In fact, due to the coupling between the two out-of-phase periodic waves, the field envelopes contain less harmonics than in the case of a single nonlinear wave, and the truncated three-wave model is more accurate for Eqs. (1) than for the scalar NLS equation. For instance, at the optimal frequency of MI, the energy content of the higher harmonics is of the order of 30% of the total field energy in the case of the NLS equation [24] while in the present case the discrepancy is only of a few percent (see Fig. 3).

The Hamiltonian formulation of the problem as given by Eqs. (6) and (7) reveals an important feature of the coupled NLS equations, namely, the existence of elliptic fixed points corresponding to steady-state solutions of these equations. These fixed points appear in Fig. 2 as the limiting states of the inner orbits for low values of H. They can be easily calculated from Eqs. (6) and (7). We find

$$\eta_e=\frac{4B-2\kappa}{8B+1},\quad \phi_e=0,\pi\ . \quad (9)$$

Naturally, the two values of the phase, $\phi=0$ and π, correspond each to circular polarization components of opposite handedness. The stationary periodic solutions thus consist of the superposition of two π out-of-phase periodic structures of counter-rotating polarizations. From Eqs. (4), (5), and (7) it is easy to see that the fixed-point

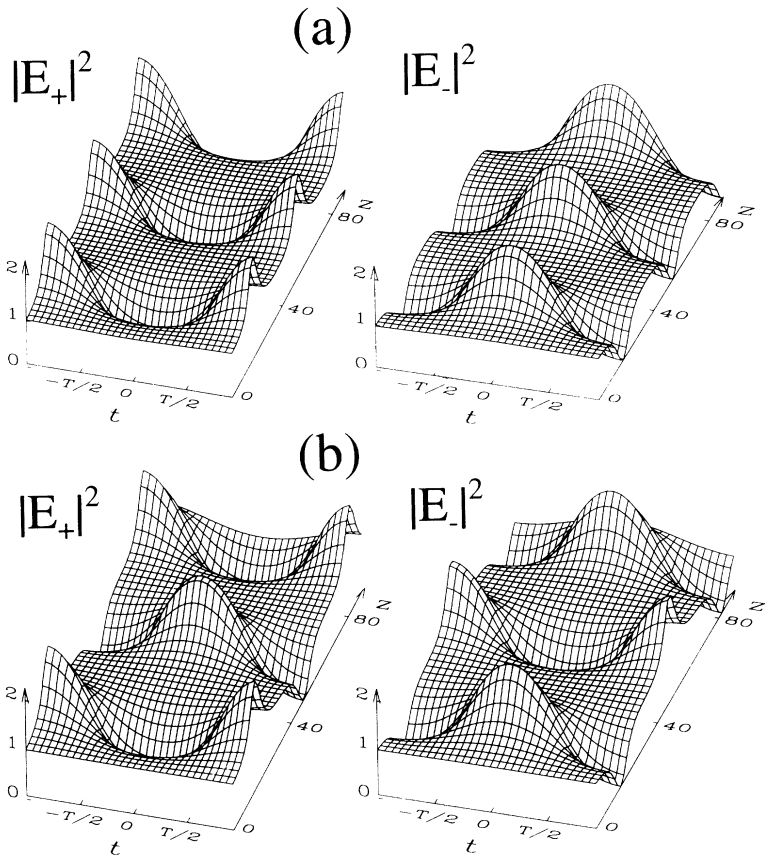

FIG. 4. Evolution of the intensity profiles of the two polarization components obtained by numerical integration of Eqs. (1). (a) The initial conditions are those of Fig. 3, i.e., it corresponds to an inner orbit of the phase-space portrait. (b) The initial condition is $E_{\pm}(z=0,t)=1\pm i\times 10^{-2}\cos(t)$, which corresponds to an outer orbit. We observe in this case the regular alternation between π out-of-phase periodic patterns predicted by the Hamiltonian model.

solutions E_+ and E_- have the form

$$E_{\pm}=[\sqrt{1-\eta_e}\pm\sqrt{2\eta_e}\cos(\Omega t)]\sqrt{P}\exp(i\beta z)\ , \quad (10)$$

where $\beta=P(1-2B\eta_e)$ is the propagation constant of the stationary periodic solution. The calculations of the absolute phase $[\exp(i\beta z)]$ of these solutions is necessary for the comparison with the exact stationary periodic solutions of Eqs. (1), which will be studied in Sec. IV. Note that the π out-of-phase envelopes of E_+ and E_- exhibit no phase variation, i.e., they are described by real functions. Figure 5 shows the envelopes $|E_+|$ and $|E_-|$ of the stationary periodic solution Eq. (10) corresponding to the elliptic fixed points of Fig. 2 (i.e., $\kappa=B=\frac{1}{3}$).

These stationary periodic solutions, which appear as limiting states of the more general space- and time-periodic solutions, are equivalent to the cnoidal waves of the NLS equation. The NLS cnoidal waves can be calculated analytically and may be expressed in terms of Jacobian elliptic functions [8]. This closed analytical form allowed the authors of Ref. [8] to establish an explicit link between MI and the bright NLS soliton, since, on the one hand, the cnoidal waves appear as limiting states of space- and time-periodic solutions, and on the other hand they tend to the one-soliton solution as their period is increased to infinity. For the coupled NLS equations (1) the situation is more difficult because no analytical solutions are known to exist. Moreover, the approximate model derived above only provides a good qualitative description of the periodic solutions of the coupled NLS equations in a limited frequency range. Ideally, in order to find the soliton associated with PMI we should look for the limiting states of the stationary periodic solutions as their period tends to infinity, or their frequency Ω tends to zero. Clearly, this cannot be done with the truncated model since a decrease of the frequency would lead to the appearance of an arbitrarily large number of higher harmonics. We then have to study numerically the stationary periodic solutions of Eqs. (1). This is the purpose of the next section. As we shall see, the information brought by the truncated Hamiltonian model greatly simplify this task.

In summary, in this section devoted to the approximat-

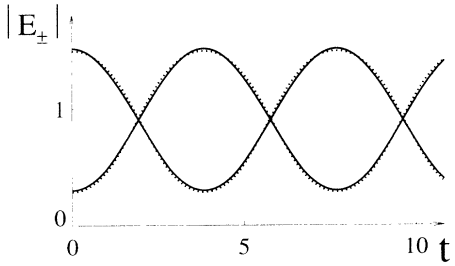

FIG. 5. Solid lines: envelopes $|E_{\pm}(z,t)|$ of the stationary periodic solutions given in Eq. (10) for the optimal frequency Ω_{2m} and $B=\frac{1}{3}$; the period is then $T=2\pi/\Omega_{2m}=7.7$. Dotted lines: stationary periodic solutions of the same frequency obtained by numerical integration of Eqs. (12) with the value of the propagation constant given by the truncated model, that is, $\beta=0.88$. The shooting parameters are $u(0)=a_{\max}=1.48$ and $v(0)=a_{\min}=0.28$.

ed three-wave model we have shown that, in the Hamiltonian representation, PMI corresponds to the existence of a hyperbolic fixed point which is itself associated with two elliptic points representing stationary periodic solutions of the coupled NLS equations. The limit in which the period of these solutions tends to infinity will then provide the soliton associated with PMI.

IV. STATIONARY PERIODIC SOLUTIONS

We now consider the exact stationary periodic solutions of the coupled NLS equations (1). These equations, being in general (i.e., for $B\neq -1$, $B\neq 0$, and $B\neq \frac{1}{2}$) nonintegrable [14,28], their solutions must be calculated numerically. The approximate model derived in Sec. III reveals that the stationary periodic solutions can be described as the superposition of two π out-of-phase periodic envelopes of counter-rotating circular polarizations. It also shows that, in a limited frequency range, these envelopes are well approximated by in-phase ($\phi=0$) or π out-of-phase ($\phi=\pi$) pump and sideband Fourier modes [see Eq. (10)]. This result is very important because it suggests that the envelopes of the stationary periodic solutions can be expressed in terms of real functions. Adopting this assumption, these solutions would then have the form [see Eq. (10)]

$$E_+ = u(t)\exp(i\beta z), \quad E_- = v(t)\exp(i\beta z) , \tag{11}$$

where the functions u and v and the propagation constant β are real quantities. Substituting Eqs. (11) into Eqs. (1) leads to a set of two coupled ordinary differential equations

$$u'' = -2\beta u + (1-B)u^3 + (1+B)v^2 u , \tag{12a}$$

$$v'' = -2\beta v + (1-B)v^3 + (1+B)u^2 v , \tag{12b}$$

where the primes denote time derivatives. From the truncated model we know that u and v are out-of-phase periodic functions. The maxima of wave u correspond then to the minima of wave v and vice versa. Choosing the time origin at one of these extrema, we can write $u'(0)=v'(0)=0$ and $u(0)=a_{\max}$, $v(0)=a_{\min}$, where $a_{\max}$ and $a_{\min}$ are the extrema of both waves. The stationary periodic solutions to Eqs. (1) can therefore be calculated by a standard shooting technique using $a_{\max}$ and $a_{\min}$ as shooting parameters. These parameters provide the initial conditions for the numerical integration of Eqs. (12). We only look for the values of $a_{\max}$ and $a_{\min}$ which lead to a periodic evolution of u and v. The dotted lines in Fig. 5 show the solution obtained from this technique for the optimal frequency Ω_{2m} and the corresponding value of the propagation constant $\beta=0.88$ predicted by the truncated model [see Eq. (10) with $B=\frac{1}{3}$ and $P=1$]. The shooting parameters are $a_{\max}=1.48$ and $a_{\min}=0.28$. As is expected for any frequency in the range $\Omega_c/2<\Omega<\Omega_c$, we verify an excellent agreement with the truncated model.

This result proves the existence of stationary periodic solutions of the form predicted by the simplified Hamiltonian model, that is, solutions composed of two π phase-shifted periodic and real envelopes in both circular polarization components. We now consider this type of solutions in the low-frequency domain which is incompatible with the Fourier-mode truncation approach.

To understand the existence and the features of the stationary periodic solutions, it is convenient to analyze Eqs. (12) in terms of a mechanical analog. Equations (12) are, in fact, the equation of motion in the plane (u,v) of a unit mass in the potential

$$V=\beta(u^2+v^2)-\tfrac{1}{4}(u^2+v^2)^2+\frac{B}{4}(u^2-v^2)^2 . \tag{13}$$

This potential possesses maxima and saddle points which correspond to fixed points of Eqs. (12). These fixed points represent naturally the steady-state cw solutions to Eqs. (1). The polarization states of these cw solutions constitute the polarization eigenstates (or eigenpolarizations) of the Kerr material [25]. Setting $u''=0$ and $v''=0$ in Eqs. (12), these solutions can be easily calculated. We find four maxima on the u and v axis,

$$(u=\pm\sqrt{2\beta/(1-B)},v=0)$$

and (14)

$$(u=0,v=\pm\sqrt{2\beta/(1-B)}) ,$$

which represent the circular eigenpolarizations. Between the maxima there are four saddle points located on the bisecting lines of the plane (u,v) which represent the linear eigenpolarizations: $u=\pm v=\beta^{1/2}$ and $u=\pm v=-\beta^{1/2}$. Note that Eqs. (12) can be normalized with respect to the parameter β by means of a simple change of variables ($t\rightarrow t/\beta^{1/2}$, $u\rightarrow u\beta^{1/2}$, $v\rightarrow v\beta^{1/2}$). For the sake of simplicity and without loss of generality we can therefore set $\beta=1$ for the study of the stationary periodic solutions.

The stationary periodic solutions studied above correspond in fact to the trajectories of the unit mass oscillating around a saddle point between two adjacent maxima. This is illustrated in Fig. 6 in which we plot the trajectories in the plane (u,v) of four stationary periodic solutions of different periods for $B=\frac{1}{3}$ [the contour lines of the potential $V(u,v)$ are included in the plots]. They were obtained from the shooting method mentioned above. For values of the ratio $a_{\max}/a_{\min}$ close to unity, i.e., for trajectories which lie in a small region around the saddle point, the frequency Ω of the oscillation is high. Whereas the trajectories obtained with large values of $a_{\max}/a_{\min}$ correspond to oscillations of low frequency. For very large periods, $T=2\pi/\Omega$, these trajectories span an angle of almost 90° in the first quadrant of the plane (u,v) and their extremities approach the maxima of the potential V.

Figure 7 shows examples of stationary periodic solutions corresponding to such trajectories at different frequencies. As the periodic increases, the amplitude $a_{\max}$ increases while $a_{\min}$ decreases, and the envelopes $u(t)$ and $v(t)$ flatten around these extrema, indicating the appearance of higher harmonics in the solutions. In Fig. 8 we plot the modulation depth, $\Delta=(a_{\max}-a_{\min})/a_{\max}$, of the envelopes as a function of their period $T=2\pi/\Omega$. We see that Δ tends to unity as the period tends to

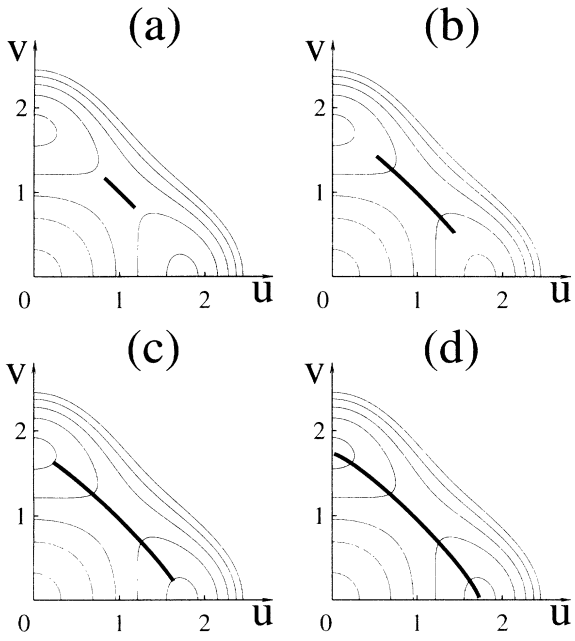

FIG. 6. Periodic trajectories in the plane (u,v) of the unit mass in the potential V obtained by numerical integration of Eqs. (11) with $B=\frac{1}{3}$ and $\beta=1$. The shooting parameters are (a) $a_{\max}=1.17$, $a_{\min}=0.82$; (b) $a_{\max}=1.43$, $a_{\min}=0.52$; (c) $a_{\max}=1.62$, $a_{\min}=0.23$; (d) $a_{\max}=1.73$, $a_{\min}=0.03$, which correspond, respectively, to the periods $T_{(a)}=5.6$, $T_{(b)}=6.2$, $T_{(c)}=7.8$, $T_{(d)}=13$.

infinity. Note that under the threshold period $T_c=5.44$ no periodic solutions are found. The existence of this threshold can be forseen from the linear stability analysis and the Hamiltonian model developed above. When the frequency Ω tends to the PMI cutoff frequency $\Omega_c=2(BP_0)^{1/2}$ of the PMI gain given in Eq. (2b), the homoclinic orbit of the Hamiltonian (6) becomes arbitrarily small and vanishes when $\Omega=\Omega_c$. Naturally, the

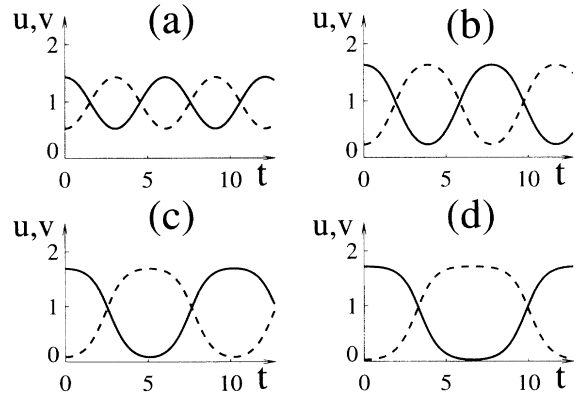

FIG. 7. Envelopes $|E_{\pm}(z,t)|$ of the stationary periodic solutions obtained by numerical integration of Eqs. (11) with $B=\frac{1}{3}$ and $\beta=1$. The shooting parameters are (a) $a_{\max}=1.43$, $a_{\min}=0.52$; (b) $a_{\max}=1.62$, $a_{\min}=0.23$; (c) $a_{\max}=1.69$, $a_{\min}=0.09$; (d) $a_{\max}=1.73$, $a_{\min}=0.03$, which correspond, respectively, to the periods $T_{(a)}=6.2$, $T_{(b)}=7.8$, $T_{(c)}=11$, $T_{(d)}=13$.

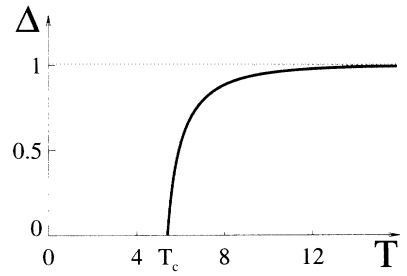

FIG. 8. Modulation depth Δ of the stationary periodic solutions as a function of their period T. A period threshold T_c is observed under which the stationary periodic solutions no longer exist. From the linear stability analysis we find $T_c=2\pi/\Omega_c$ which, for $B=\frac{1}{3}$ and $\beta=1$ considered here, gives $T_c=5.44$.

corresponding fixed points given in Eq. (9) (with $\kappa\to 2B$) tend to the origin or, in other words, the stationary periodic solutions tend to a stable cw solution and $\Delta\to 0$. It is easy to verify that the threshold periodic corresponds, in agreement with this reasoning, to the cutoff frequency, that is, $T_c=2\pi/\Omega_c$. In fact, with the choice $\beta=1$, the power P_0 of the cw solution (saddle point of V) is unity, so that, $T_c=\pi/(B)^{1/2}$ which, in the case $B=\frac{1}{3}$, gives $T_c=5.44$ in agreement with Fig. 8.

Figure 7 shows that in the other limit, at very low frequency, the stationary periodic solutions consist of an alternation between quasi-cw domains of counter-rotating circular polarizations. Each domain is separated from one another by a localized structure in which the polarization switches from one circular state to the other. As the frequency Ω tends to zero, or in other words when the distance, $T=2\pi/\Omega$, between these localized structures becomes infinite, the envelopes u,v take the form of two symmetric semi-infinite kink waves. The localized structure they form appears then as a solitary wave exactly as the NLS soliton constitutes the limiting state of the cnoidal waves. Consequently, we can interpret the localized structure of this limit as being the soliton associated with PMI in the coupled NLS equations. The next section is devoted to a detailed analysis of these new fundamental solutions to Eqs. (1).

V. SOLITON ASSOCIATED WITH PMI

The solitary-wave solutions of Eqs. (1) correspond to the separatrix trajectories of the potential V, i.e., the trajectories in the plane (u,v) that connect pairs of saddle points or maxima. The separatrices that connect opposite maxima correspond naturally to the circularly polarized NLS dark solitons. Setting $v=0$ and $u=0$ in Eqs. (12a) and (12b), respectively, we find

$$u=\sqrt{2\beta/(1-B)}\tanh(\sqrt{\beta}t),\quad v=0$$

and (15)

$$u=0,\quad v=\sqrt{2\beta/(1-B)}\tanh(\sqrt{\beta}t)\ .$$

The separatrices that connect the pairs of opposite saddle points lie on the bisecting lines $u=\pm v$ and correspond to the linearly polarized NLS dark solitons. Setting $u=\pm v$

in Eqs. (11) yields $u=\pm v=\sqrt{\beta}\tanh(\sqrt{\beta}t)$.

In Fig. 9 we show a contour plot of the potential $V(u,v)$ in the case where $B=\frac{1}{3}$. As in Sec. IV, for the sake of simplicity we only consider the value $\beta=1$ [normalization of Eqs. (12) with respect to β]. The maxima of V are then located in $(u=\pm\sqrt{3},v=0)$ and $(u=0,v=\pm\sqrt{3})$. The thick lines on the axis in Fig. 9 connect opposite maxima and correspond to the circularly polarized NLS dark solitons. The dashed lines which connect opposite saddle points are the separatrices of the linearly polarized dark solitons. From that simple mechanical analog picture of the problem it is easy to see that another type of solitary wave must exist that corresponds to the separatrix trajectories that connect adjacent maxima of the potential. These trajectories can easily be calculated numerically using the shooting method mentioned above for the study of the periodic solutions. The dotted lines in Fig. 9 show the four separatrices that connect the four adjacent maxima of V. The envelopes $u(t)$ and $v(t)$ of the separatrix of the first quadrant are shown in Fig. 10. These solitary waves naturally correspond to the PMI soliton, i.e., the limiting state of the stationary periodic solutions studied in Sec. IV [see Figs. 6(d) and 7(d)].

In Fig. 11 we plot the envelopes u,v of the separatrix of the second quadrant $(u<0,v>0)$. We see that, contrary to the waves of Fig. 10, these envelopes are not mirror images of one another. We cannot therefore see them as the limiting state of two identical but out-of-phase periodic structures of opposite polarizations. In fact, it is easy to show that these waves also constitute the soliton associated with PMI. The only difference with the analysis above is that one must now consider PMI of a linearly polarized continuous wave which has a polarization orthogonal to that considered in Sec. II. In that section we studied PMI of a linearly polarized cw field by assuming identical circular polarization components $E_+=E_-$. Introducing the linear polarization components $E_x=(E_++E_-)/\sqrt{2}$, and $E_y=(E_+-E_-)/i\sqrt{2}$, we see that we have implicitly considered a linear

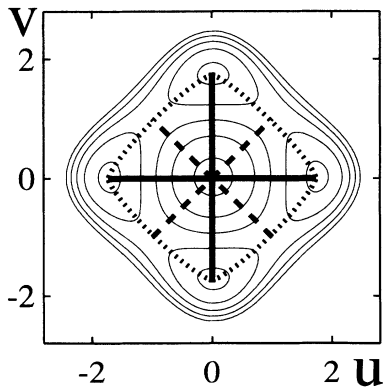

FIG. 9. Contour plot of the potential V in the (u,v) plane for $B=\frac{1}{3}$ and $\beta=1$. The solid and dashed lines show the separatrices of the circularly and linearly polarized NLS dark solitons, respectively. The dotted lines connect the four adjacent maxima of the potential. They are the separatrices of the solitons associated with PMI.

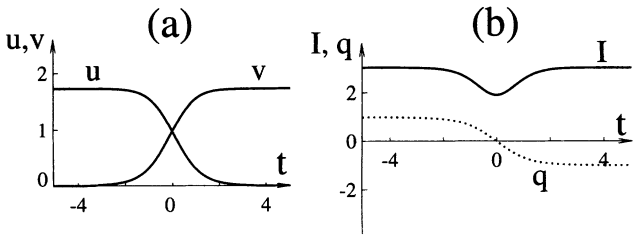

FIG. 10. (a) Circular polarization envelopes $u(t)$ and $v(t)$ of the PMI soliton corresponding to the separatrix of the first quadrant $(u,v>0)$ shown in Fig. 9. (b) Total intensity profile $I(t)$ and ellipticity degree $q(t)$ of the PMI soliton [q is the ratio between the short and long axes of the polarization ellipse $q=(u-v)/(u+v)$].

polarization parallel to the x axis. Since we only deal here with isotropic Kerr media, this choice is obviously arbitrary and we could have considered for example a polarization parallel to the y axis. In that case we would have had $E_-=-E_+$, and the analysis above would have lead to the ansatz $E_\pm=\pm E_0+\sqrt{2}E_1\cos(\Omega t)$ instead of Eq. (3). It is then easy to see from the symmetry of Eqs. (1) that, with this new ansatz, the truncation procedure leads to the same Hamiltonian model (6) and (7). The fixed points of the Hamiltonian represent now counterrotating waves which exhibit identical periodic modulation on background waves of opposite amplitudes. Clearly, the limiting state of the corresponding stationary periodic solutions is in this case the solitary wave shown in Fig. 11. The solitary waves of the separatrices of the third and fourth quadrants are equivalent to those of the first and second quadrants, respectively, since they involve a change of sign in both circular components.

In Figs. 10 and 11 we also plot the total intensity profile $I=u^2+v^2$ and the ellipticity degree q (ratio between the short and long axes of the polarization ellipse) of the PMI soliton. The values $q=\pm1$ represent opposite circular polarizations while $q=0$ represents a linear polarization. Note that, since u and v are real functions, the axes of the polarization ellipse retain the same orientation across the entire localized structure. Because its intensity profile exhibits a dip on a constant background, the PMI soliton constitutes a vector solitary wave of the dark type. Figures 10(b) and 11(b) show that the intensity dip is accompanied by a variation of the ellipticity degree of

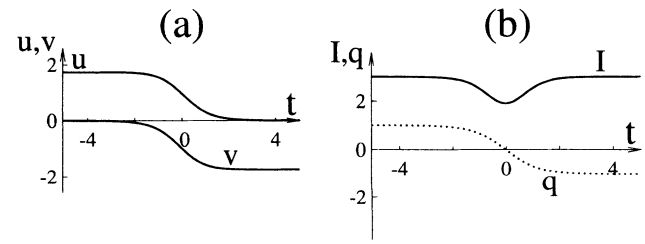

FIG. 11. (a) Circular polarization envelopes $u(t)$ and $v(t)$ of the PMI soliton corresponding to the separatrix of the second quadrant $(u<0,v>0)$ shown in Fig. 9. (b) Total intensity profile $I(t)$ and ellipticity degree $q(t)$ of the PMI soliton [here we have $q=(u+v)/(u-v)$].

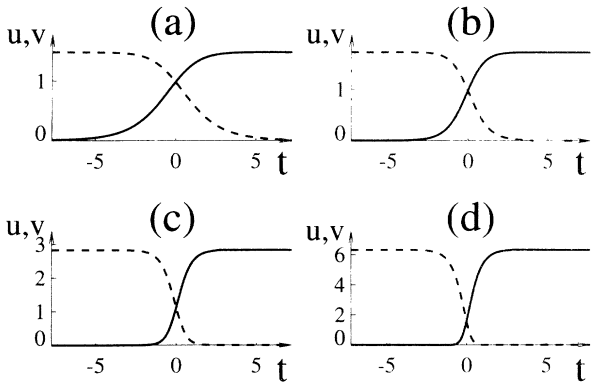

FIG. 12. Illustration of the influence of the parameter B on the PMI soliton. (a) $B=0.1$, (b) $B=0.33$, (c) $B=0.75$, (d) $B=0.95$.

the field between two constant values. Notice that a circularly polarized wave is modulationally stable in the normal-dispersion regime. We can then say that the PMI soliton separates two semi-infinite domains of orthogonal stable eigenpolarizations of the Kerr medium. From that point of view and by analogy to the theory of ferromagnetism, the new soliton can be interpreted as a polarization domain wall (the atomic spin being replaced here by the polarization of light). Note that this terminology has already been used in nonlinear optics to qualify the localized structure which may occur in two polarized beams counterpropagating in a dispersionless Kerr medium [37,38].

Let us now consider the influence of the parameter B on the PMI solitons. It is easy to see from Eq. (13) that, when $B=0$, the potential V has a circular symmetry and no longer possesses maxima or saddle points. This means that the existence and features of the PMI solitons directly depends on the tensor character of the Kerr nonlinearity. Figure 12 illustrates the influence of B on the soliton. We see that a decrease of B leads to an increase of the soliton width and a decrease of the intensity dip. In the limit $B\rightarrow 0$ the width tends to infinity and, in other words, the soliton no longer exists. This result is in agreement with the study of PMI of Sec. II in which we showed that when $B\rightarrow 0$ the PMI gain and the corresponding frequency tend to zero (i.e., the period of modulation becomes infinite). In the other limit, as B tends to unity the soliton width decreases while its intensity minimum approaches zero.

VI. CONCLUSIONS

In this paper we studied modulational instability and the periodic solutions of the incoherently coupled NLS equations which govern light propagation in isotropic Kerr materials. We derived from these equations a simplified approximate Hamiltonian model which was shown to provide a good qualitative picture of the dynamics of PMI and periodic solutions. In particular, this model predicts a recurrent behavior analogous to that observed in the NLS equation (Fermi-Pasta-Ulam recurrence). Another important prediction of the Hamiltonian model is the existence of stationary periodic solutions in the form of identical but out-of-phase periodic and real envelopes in the two circular polarization components. This result has been confirmed by the numerical study of the exact stationary periodic solutions of the coupled NLS equations. We showed numerically that the family of stationary periodic solutions tends to a solitary-wave solution as the period is increased to infinity. This solitary wave was thus identified as the soliton associated with PMI in the normal dispersion regime. A mechanical analog approach to the problem allowed us to perform a detailed analysis of this new fundamental nonlinear wave of isotropic Kerr materials. We showed that the PMI soliton constitutes a new type of vector dark soliton which can be viewed as a polarization domain wall.

From a more general point of view, our analysis demonstrates the existence, conjectured by Agrawal in 1987 [10], of the soliton associated with modulational instability induced by cross-phase-modulation in the normal dispersion regime. For the sake of simplicity we restricted the problem to that of copropagating polarized laser pulses for which XPM is related to the tensor character of the Kerr nonlinearity. However, XPM being a general feature characteristic of the simultaneous propagation of two waves belonging to different optical modes, our analysis is liable to apply to other physical situations. In particular, as mentioned in Sec. II, our results can be directly adapted to the spatial domain for the problem of transverse modulational instability and pattern formation in the profile of two-dimensional polarized beams in defocusing Kerr media. We believe that an extension of the present theory to the more general case of birefringent Kerr materials is possible. In that case the PMI soliton would appear as a localized structure separating domains of elliptical polarizations which constitute the nonlinear eigenpolarizations of the material. The experimental observation of the soliton associated with modulational instability in the normal-dispersion regime would be of great interest since it constitutes a new fundamental phenomenon of nonlinear wave dynamics.

ACKNOWLEDGMENTS

The authors acknowledge fruitful discussions with Yu. S. Kivshar and N. N. Akhmediev. This work was supported by the Australian Photonics Cooperative Research Centre (APCRC).

[1] A. Hasegawa, *Plasma Instabilities and Nonlinear Effects* (Springer-Verlag, Heidelberg, 1975).

[2] See, e.g., T. J. Benjamin and J. E. Feir, J. Fluid Mech. **27**, 417 (1967).

[3] See, e.g., G. P. Agrawal, *Nonlinear Fiber Optics* (Academic, New York, 1989), and references therein.

[4] V. E. Zakharov and A. B. Shabat, Zh. Eksp. Teor. Fiz. **61**, 118 (1971) [Sov. Phys. JETP **34**, 62 (1972)].

[5] A. Hasegawa and F. Tappert, Appl. Phys. Lett. **23**, 142 (1973).
[6] A. Hasegawa and W. F. Brinkman, IEEE J. Quantum Electron. **QE-16**, 694 (1980).
[7] N. N. Akhmediev and V. I. Korneev, Teor. Mat. Fiz. **69**, 189 (1986) [Teor. Math. Phys. **69**, 1089 (1986)].
[8] N. N. Akhmediev, V. M. Eleonskii, and N. E. Kulagin, Teor. Mat. Fiz. **72**, 183 (1987) [Theor. Math. Phys. **72**, 809 (1987)].
[9] A. L. Berkoer and V. E. Zakharov, Zh. Eksp. Teor. Fiz. **58**, 903 (1979) [Sov. Phys. JETP **31**, 486 (1970)].
[10] G. P. Agrawal, Phys. Rev. Lett. **59**, 880 (1987).
[11] D. N. Christodoulides and R. I. Joseph, Opt. Lett. **13**, 53 (1988).
[12] M. V. Tratnik and J. E. Sipe, Phys. Rev. A **38**, 2011 (1988).
[13] N. N. Akhmediev, V. M. Eleonskii, N. E. Kulagin, and L. P. Shil'nikov, Pis'ma Zh. Tekh. Fiz. **15**, 19 (1989) [Sov. Tech. Phys. Lett. **15**, 587 (1989)].
[14] V. M. Eleonskii, V. G. Korolev, N. E. Kulagin, and L. P. Shil'nikov, Zh. Eksp. Teor. Fiz. **99**, 1113 (1991) [Sov. Phys. JETP **72**, 619 (1991)].
[15] R. J. Dowling, Phys. Rev. A **42**, 5553 (1990).
[16] M. Haelterman and A. P. Sheppard, Electron. Lett. **29**, 1176 (1993).
[17] M. Haelterman, A. P. Sheppard, and A. W. Snyder, Opt. Lett. **18**, 1406 (1993).
[18] D. N. Christodoulides, Phys. Lett. A **132**, 451 (1988).
[19] S. Wabnitz, E. M. Wright, and G. I. Stegeman, Phys. Rev. A **41**, 6415 (1990).
[20] S. Trillo, S. Wabnitz, E. M. Wright, and G. I. Stegeman, Opt. Lett. **13**, 871 (1988).
[21] V. V. Afanasyev, E. M. Dianov, and V. N. Serkin, IEEE J. Quantum Electron. **QE-25**, 2656 (1989).
[22] M. V. Tratnik, Opt. Lett. **17**, 917 (1992).
[23] Yu. S. Kivsar and S. K. Turitsyn, Opt. Lett. **18**, 337 (1993).
[24] E. Infeld, Phys. Rev. Lett. **47**, 717 (1981).
[25] P. D. Maker and R. W. Terhune, Phys. Rev. A **137**, 801 (1965).
[26] S. Trillo and S. Wabnitz, J. Opt. Soc. Am. B **6**, 238 (1989).
[27] *Handbook of Mathematical Functions*, edited by M. Abramowitz and I. A. Stegun (Dover, New York, 1970), Chap. 16, p. 571.
[28] V. E. Zakharov and E. I. Schulman, Physica D **4**, 270 (1982).
[29] N. N. Akhmediev, V. I. Korneev, and Yu. V. Kuz'menko, Zh. Eksp. Teor. Fiz. **88**, 107 (1985).
[30] S. Trillo and S. Wabnitz, Opt. Lett. **16**, 986 (1991).
[31] G. Cappellini and S. Trillo, J. Opt. Soc. Am. B **8**, 824 (1991).
[32] S. Trillo and S. Wabnitz, Opt. Lett. **16**, 1566 (1991).
[33] M. Haelterman, S. Trillo, and S. Wabnitz, Opt. Lett. **17**, 745 (1992).
[34] M. Haelterman, S. Trillo, and S. Wabnitz, Opt. Commun. **93**, 343 (1992).
[35] M. Haelterman, S. Trillo, and S. Wabnitz, Phys. Rev. A **47**, 2344 (1993).
[36] S. Trillo and S. Wabnitz, Phys. Lett. A **159**, 252 (1991).
[37] V. E. Zakharov and A. V. Mikhailov, Pis'ma Zh. Eksp. Teor. Fiz. **45**, 279 (1987) [JETP Lett. **45**, 349 (1987)].
[38] D. David, D. D. Holm, and M. V. Tratnik, Phys. Rep. **187**, 281 (1990).